Spatial-spectral coupling in hyperspectral CARS microscopy image formation

Aaron M. Barlow[a,b], Konstantin Popov[b], Marco Andreana[a,b], Douglas J. Moffatt[b], Andrew Ridsdale[b], Aaron D. Slepkov[c], Lora Ramunno[b], and Albert Stolow[a,b,d]

[a]SDT, Emerging Technologies Division, National Research Council of Canada, 100 Sussex Dr., Ottawa ON, Canada;
[b]Department of Physics, University of Ottawa, Ottawa ON, Canada;
[c]Department of Physics & Astronomy Trent University, Peterborough ON, Canada;
[d]Department of Physics, Queen's University, Kingston ON, Canada

ABSTRACT

Hyperspectral coherent anti-Stokes Raman scattering (CARS) microscopy has provided an imaging tool for extraction of 3-dimensional volumetric information, as well as chemically-sensitive spectral information. These techniques have been used in a variety of different domains including biophysics, geology, and material science. The measured CARS spectrum results from interference between the Raman response of the sample and a non-resonant background. We have collected four dimensional data sets (three spatial dimensions, plus spectra) and extracted Raman response from the CARS spectrum using a Kramers-Kronig transformation. However, the three dimensional images formed by a CARS microscope are distorted by interference, some of which arises because of the Gouy phase shift. This type of interference comes from the axial position of the Raman resonant object in the laser focus. We studied how the Gouy phase manifests itself in the spectral domain by investigating microscopic diamonds and nitrobenzene droplets in a CARS microscope. Through experimental results and numerical calculation using finite-difference time-domain (FDTD) methods, we were able to demonstrate the relationship between the spatial configuration of the sample and the CARS spectral response in three dimensional space.

Keywords: Coherence imaging, Nonlinear microscopy, Raman spectroscopy, CARS Microscopy

1. INTRODUCTION

Coherent anti-Stokes Raman scattering (CARS) is a non-linear optical process that has attracted considerable attention in applications as wide-ranging as biophysics,[1] material science,[2] and geology.[3] The versatility of CARS owes to the fact that it probes specific vibrational resonances in molecules that are essentially equivalent to spontaneous Raman spectroscopy, with the added advantage of being a coherent, stimulated process, resulting in much stronger signals.[4] When combined with a conventional confocal microscope, CARS may be used to produce label-free, frequency-resolved three-dimensional volumetric images of microscopic objects,[5] and many such implementations are able to simultaneously probe other non-linear signals such as two-photon fluorescence and second harmonic generation in multi-modal CARS imaging.[6]

One major drawback to the CARS process is the presence of a non-resonant background (NRB), which results in distortions of the CARS spectrum. The non-resonant background arises from the interaction between the laser and the medium in which the sample is embedded, and interferes coherently with the resonant CARS response.[7] In particular, a typical CARS spectrum has its peak shifted relative to the spontaneous Raman response, and a characteristic dip in signal below the background.[8] For applications where the spectrum is crowded with many resonances in close proximity, such as in the spectral "fingerprint" region (500-2000 cm^{-1}), these distortions can greatly increase the challenge in correctly assigning the vibrational resonance to a particular

Further author information:
Aaron M. Barlow: E-mail: aaron.barlow@nrc-cnrc.gc.ca,
Konstantin Popov: E-mail: kpopov@uottawa.ca

Three-Dimensional and Multidimensional Microscopy: Image Acquisition and Processing XX,
edited by Carol J. Cogswell, Thomas G. Brown, Jose-Angel Conchello, Tony Wilson, Proc. of SPIE Vol. 8589,
85890T · © 2013 SPIE · CCC code: 1605-7422/13/$18 · doi: 10.1117/12.2004217

species. Consequently, techniques have been developed to separate the resonant and non-resonant components of the CARS response and retrieve the spontaneous Raman spectrum such as the Kramers-Kronig relations[9] and the maximum entropy method.[10] Such methods have been used to provide detailed information about the localized chemical, physical, or thermodynamic state of a system resulting from spectral variations in specific regions a sample.[11–13]

Because CARS is a coherent process, there is also the possibility that artifacts may arise owing to interference effects as the signal propagates through the sample. Shadows have been identified in CARS images that are associated with such interference effects,[14,15] including index-mismatch,[16] and most recently, the Gouy phase shift.[17] Such artifacts are quite localized, typically only associated with regions of interest on the scale of the Rayleigh range of the laser focus. As we demonstrate in this report, corresponding distortions in the spectral domain on the order of the spectral linewidth are possible as a result of phase shifts resulting from the propagation of the CARS response and an inherent spatial-spectral coupling is present in such experiments.

This paper is organized as follows: In Section 2, we briefly review the theoretical assumptions underlying the collection of CARS signals and the subsequent retrieval of the resonant Raman spectrum, and explain how shifts in the phase resulting from the Gouy phase or index-mismatch may result in spatial and spectral distortions. In Section 3, we outline the experimental technique used to demonstrate the spectral shifts, and the accompanying simulation methodology. In Section 4, we show the results of our experiments and numerical simulations. In Section 5, we discuss the consequences of our results and comment on avenues by which these difficulties may be alleviated.

2. THEORY

CARS is a coherent four-wave mixing process resulting from the third-order non-linear susceptibility $\chi_R^{(3)}(\omega)$ associated with a vibrational resonance Ω_R. The process is characterized by an absorption of a pump photon at frequency ω_p, followed by a stimulated resonant emission induced by a Stokes photon at frequency ω_S onto the Raman vibration of interest, Ω_R. A subsequent excitation using a second pump photon ω_p leads to an emission of a blue-shifted anti-Stokes photon with frequency $\omega_{as} = 2\omega_p - \omega_S$. A similar four-wave mixing process produces a non-resonant signal at the same frequency as the desired anti-Stokes light that is coherent with the resonant response, producing a non-resonant background that interferes with the resonant signal. Specifically, intensity of the light in the far field is given by the square modulus of the (real) non-resonant and (imaginary) resonant contributions as shown in Equation 1,

$$I_{CARS}(\omega) \propto |\chi^{(3)}(\omega)|^2 = |\chi_{NR}^{(3)} + \chi_R^{(3)}(\omega)|^2 = |\chi_R^{(3)}|^2 + |\chi_{NR}^{(3)}|^2 + 2\chi_{NR}^{(3)} Re(\chi_R^{(3)}) \tag{1}$$

where $\chi_{NR}^{(3)}$ is the susceptibility of the non-resonant background. The interference between the resonant and non-resonant signals produces a spectrum which is distorted[7] relative to that of the spontaneous Raman response. The resonant signal can be extracted directly from the combined signal, using retrieval algorithms such as those based on the Kramers-Kronig relations.[9] The Kramers-Kronig method allows extraction of the spectral phase $\phi(\omega)$ from the modulus of the susceptibility through Equation 2,

$$\phi(\omega) = -\frac{P}{\pi} \int_{-\infty}^{\infty} \frac{\ln|\chi(\omega'')|}{\omega'' - \omega} d\omega \tag{2}$$

where $\chi(\omega) = |\chi(\omega)| \exp(i\phi(\omega))$ and P is the Cauchy principal value. Once the spectral phase is known, the resonant contribution can be extracted directly via $\chi_R^{(3)} = \mathrm{Im}(\chi(\omega))$

Equation 1 describes the observed signal as a coherent sum of the purely real non-resonant response, and the purely imaginary resonant response; however, if the resonant response is shifted by an arbitrary phase $\delta\phi$, then the resonant response will no longer be purely imaginary. This phase shift will result predominately from the Gouy phase of the pump (ϕ_{Gp}) and Stokes beams ϕ_{Gs}, but further phase distortions may result from linear index-mismatch between the sample and background medium ($\delta\phi_l$), and possibly other effects. The total phase shift may therefore be written in terms of these quantities as shown in Equation 3.

$$\delta\phi = 2\phi_{Gp} - \phi_{Gs} + \delta\phi_l \tag{3}$$

Equation 1 must therefore be modified to account for the additional phase shift, as shown in Equation 4.

$$I_{CARS}(\omega) \propto |\chi^{(3)}(\omega)|^2 = |\chi_R^{(3)}|^2 + |\chi_{NR}^{(3)}|^2 + 2\chi_{NR}^{(3)} Re(\chi_R^{(3)} e^{i\delta\phi}) \tag{4}$$

As discussed in Section 4, failure to account for this additional phase contribution will lead to undesirable artifacts (spatial-spectral coupling) that will persist in commonly-used Raman retrieval methods.

3. EXPERIMENTAL METHODS

Our experimental setup for performing CARS measurements in the fingerprint region (1000 cm^{-1} to 1650 cm^{-1}) has been described in detail elsewhere.[18] In brief, we tuned our Coherent Mira900 oscillator to a wavelength of 900nm, yielding a power of ∼500 mW after a prism compressor. The light was split into two arms corresponding to the pump and Stokes. The light in the Stokes arm was directed into an NKT FemtoWhite photonic crystal fibre to produce a supercontinuum, which was filtered to remove the visible components. The pump and Stokes light were chirp-matched using SF_6 glass to achieved so-called "spectral-focusing".[19] The beams were recombined and propagated into an Olympus Fluoview 300 laser scanning microscope with powers of ∼150mW and ∼20 mW in pump and Stokes, respectively.

We examined two prototypical samples to illustrate the limiting cases of large and small Raman cross-sections. One sample consisted of microscopic diamonds of size $\sim 2\mu$m in aqueous solution. Diamond has a characteristic Raman resonance at 1334 cm^{-1} with a typical spectral width of ∼4 cm^{-1}, and this peak has among the strongest Raman responses of any homogenous sample,[20] and is therefore appropriate to treat the case of $\chi_R^3 >> \chi_{NR}^3$. The diamonds were immersed in a solution of 1% agarose at a 1 to 25 ratio at 80^{o}C to form a gel. The second sample consisted of a dilute solution of nitrobenzene in agarose. Nitrobenzene has a weak Raman resonance at 1585 cm^{-1}, corresponding to the C=C stretch mode.[21] In this case, the resonant to non-resonant response is ∼2:1, and there will be appreciable signal from the cross-term between the resonant and non-resonant responses noted in Equation 1. The nitrobenzene was mixed into the agarose at 80^{o}C with vigorous stirring to create a gel with a distribution of droplets of sizes ∼1 μm to ∼ 10 μm.

We simulated our model system of nitrobenzene immersed in the aragose medium using a three dimensional finite-difference time-domain code.[17] An isolated droplet of diameter 1 μm was set on the laser axis within a NRB of similar magnitude to the resonant response. The Raman frequency is $\Omega_R = 1600$ cm^{-1} (0.144 ω_p, where ω_p is the pump frequency), the line width is $\Gamma = 15$ cm^{-1} (1.34 $\times 10^{-3}\omega_p$), and the system is described by the third-order Raman polarization.[22] The medium was assumed to be homogenous with a linear refractive index of $n_0 = 1.34$ and a nonzero Kerr suspectibility that accounts for the non-resonant signal. The pump wavelength was chosen to be 900 nm and the Stokes was redshifted by a frequency ω. Both pulse widths were 2 ps. Within the simulation domain, the signal was propagated by a standard Maxwell solver,[23] modified to account for the proper constitutive relations due to the nonlinear media.[22] The simulation domain has radiation absorbing boundary conditions. The anti-Stokes signal is measured near the boundary of simulation domain and is further propagated analytically to the far-field zone by a near-to-far field transformation, where it is measured.

4. RESULTS

A CARS image of the diamonds at a particular focus ($z = 0\mu$ m) is shown in Figure 1a, and the image of nitrobenzene at the best focus of the highlighted droplet is shown in Figure 1b. The CARS spectra of the highlighted diamond and nitrobenzene droplets are shown in Figure 2a and 2b, respectively, at three different focii corresponding to the laser focused in front of the sample ($z = -1\mu$m), at best focus ($z = 0\mu$m) and behind the sample ($z = 1\mu$m). While the CARS image of the diamonds has a relatively homogenous background, numerous shadows may be seen in the image of the nitrobenzene associated with out-of-focus droplets. We note that while the nitrobenzene displays the familiar redshift of the peak and characteristic dip in the CARS signal, the diamond does not display these features. Rather, the diamond spectrum closely resembles the spontaneous Raman spectrum, broadened due to the spectral resolution of our spectral focus, ∼30 cm^{-1}. Moreover, we

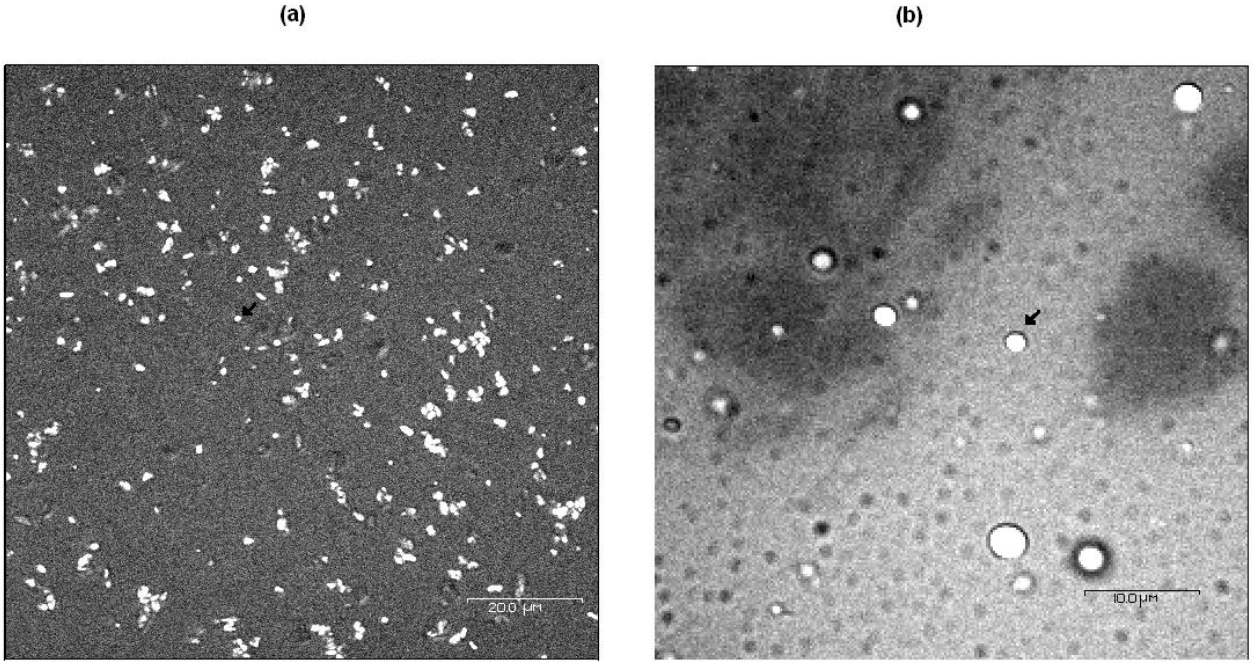

Figure 1. CARS image of (a) diamond fragments and (b) nitrobenzene droplets at best focus. Note the presence of the shadows of out of focus objects projected into the image plane.

note that there is significant distortion of the CARS spectrum of the nitrobenzene droplets depending on the focal position, whereas the diamond spectrum is relatively insensitive to position of the laser focus. It must be stressed that the three spectra in Figure 2b are all associated with the same homogenous nitrobenzene droplet: Any spectral distortions are due entirely to optical effects, and not due to the composition of the droplet, which is uniform. The simulated CARS spectra of the nitrobenzene drops are plotted in Figure 2c. For simplicity of analysis, the resonant and non-resonant media were index-matched in this case, corresponding to the case of $\delta\phi_l = 0$. Importantly, the simulated spectra at $z = 1$ μm and $z = -1$ μm are not identical, suggesting that this is indeed a propagation effect that depends on the orientation of the laser axis, similar to the asymmetry associated with observed shadows due to the Gouy phase.[17] For a more complete picture of the effects of the phase, we include the relative index mismatch between nitrobenzene ($n = 1.554$) and agarose ($n = 1.33$) in the simulations in Figure 2b, revealing further distortions in the CARS spectrum even at best focus.

These spectral shifts cannot be accounted for using standard Raman retrieval algorithms. The Raman spectra of the nitrobenzene as retrieved using a Kramers-Kronig algorithm[9] are shown in Figure 3a. The spectral peak shifts by as much as 10 cm^{-1} as the laser focus scans through the sample, and only at best focus will the retrieved Raman peak match that of the spontaneous Raman. For the simulations, a simple retrieval routine suitable for a single isolated peak in a slowly-varying NRB was developed to retrieve the Raman spectrum from the simulated data using a simulated annealing search,[24] with the Raman resonance assumed to be in the form of a Lorentzian of the form of Equation 5 with resonant susceptibility $\chi^{(3)}_{R0}$.

$$\chi^{(3)}_R(\omega) = \chi^{(3)}_{R0}\frac{\Gamma}{\Omega_R - \omega - i\Gamma} \tag{5}$$

This simplified retrieval routine allows us to account directly for the phase shift $\delta\phi$. The results of the retrieval with explicitly assumed $\delta\phi = 0$ are shown in Figure 3b. It is clear that, in this case, the phase retrieval does not reproduce the spontaneous Raman spectrum faithfully, but instead produces a shift in the peak based on the position of the droplet within the focal plane of order the spontaneous linewidth, 10 cm^{-1}. This observed shift is consistent with the results of the experimental measurements seen in Figure 3a. When the model is allowed to

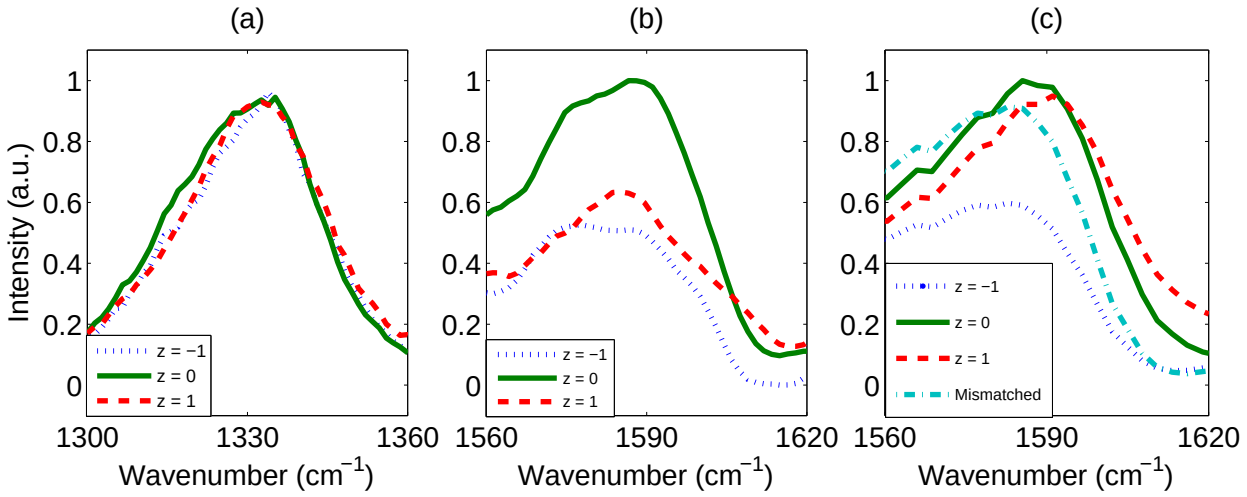

Figure 2. (a) Experimentally measured CARS spectra of the diamond fragments located at best focus ($z = 0$, solid line) and slightly off-focus ($z =$ -1 μm, dashed line, and $z = +1$ μm, dotted line) (b) Experimentally measured CARS spectra of the nitrozbenzene droplets at the best focus and slightly off-focus. (c) Calculated CARS spectra of nitrobenzene using FDTD at best focus, slightly off-focus, and at $z = 0$ with the index mismatch between nitrobenzene and agarose accounted for (partial dashes)

fit $\delta\phi$ as a free parameter, the shift vanishes, and the peak position is consistent at all three laser focal positions, as seen in Figure 3c. By construction, the only factor available to contribute to the phase shift in this case is the Gouy phase. Thus not only is the Gouy phase responsible for imaging artifacts in the spatial domain, but is also responsible for coupled distortions in the spectral domain.

5. DISCUSSION

The two samples under observation have notable differences in the generated spectra. In the case of diamond, the spectrum is essentially identical to the spontaneous Raman spectrum as seen in Figure 2a. In fact, even the standard spectral distortion normally associated with CARS spectra is not present in this case: the CARS spectrum is essentially equivalent to the spontaneous Raman even without retrieval. This may be attributed to the fact that the resonant $\chi_R^{(3)}$ of the diamond is many times stronger than the non-resonant background $\chi_{NR}^{(3)}$. Consequently, the resonant term dominates in Equation 1, and the other terms may be safely neglected as small perturbations of the signal. Thus, in this regime, the resonant and non-resonant signals are essentially decoupled. By contrast, in the case of the nitrobenzene, the CARS spectrum of the droplet varies significantly as it is moved away from the focal plane, and this effect persists into the retrieved spectrum, resulting in a notable shift in the spectral peak.

The spatial-spectral couplings and distortions may be attributed to the phase shift introduced by the Gouy phase. The simulations reveal that a retrieval algorithm using Equation 1–which is unaware of the phase shift $\delta\phi$–will retrieve a Raman spectrum has a spectral shift of order the spontaneous Raman linewidth as shown in Figure 3b, consistent with the experiment measurements. Conversely, when the retrieval algorithm instead uses Equation 4 as in Figure 3c, the recovered spectral peak is consistent at all focal positions. This problem is further exacerbated by the introduction of a phase shift resulting from refractive index mismatch as shown in Figure 2c.

The experimental results clearly demonstrate that there are two regimes that must be considered when analyzing a CARS spectrum and its corresponding retrieved Raman spectrum. In the limit of large resonant signals, such as the diamond resonance, the spectral distortions will be minimal, and the CARS spectrum and

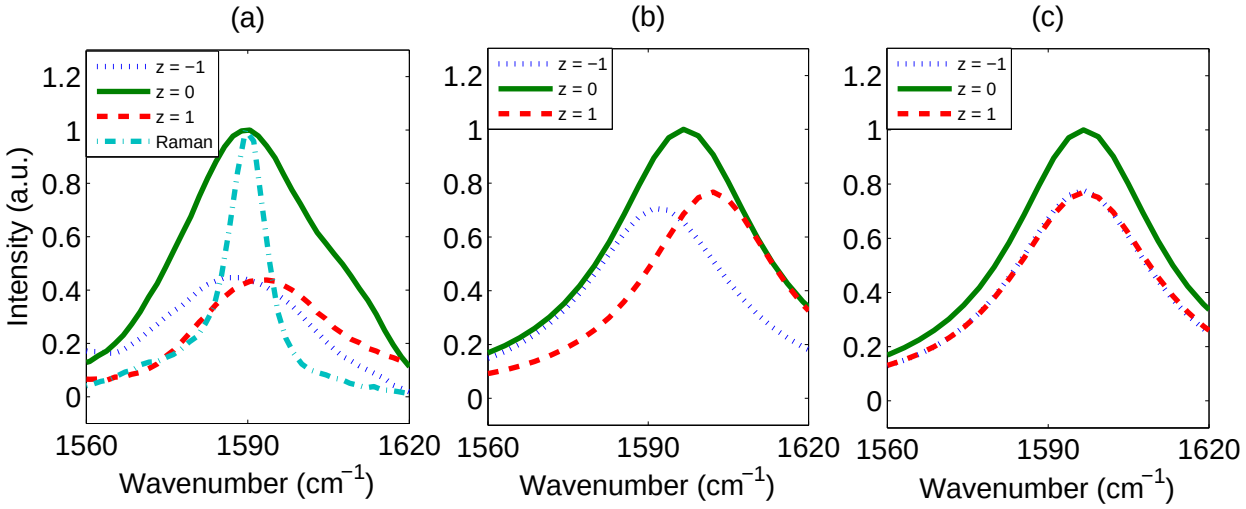

Figure 3. (a) Raman spectrum of experimental nitrobenzene droplets as retrieved through Kramers-Kronig algorithm (z = -1 μm, dashed line, and z = +1 μm, dotted line), overlaid with the spontaneous Raman spectrum (partial dashes). (b) Raman spectra of calculated nitrobenzene spectrum retrieved through simulated annealing search from the nitrozbenzene droplets at the best focus and slightly off-focus with $\delta\phi = 0$. (c) Raman spectra of calculated nitrobenzene spectrum retrieved through simulated annealing search from the nitrozbenzene droplets at the best focus and slightly off-focus with $\delta\phi$ as a free parameter.

Raman spectrum will be essentially equivalent. In the limit of small resonant signals, there will be significant spatial-spectral coupling between the resonant response and the non-resonant background. This coupling will manifest itself simultaneously as shadows in the image and distortions in the spectrum. There artifacts will considerably complicate the analysis of CARS images and their spectra if they cannot be corrected for. Assigning physical significance to regions that are darkened in an image may in fact be the result of out-of-focus objects producing shadows in the focal plane; likewise, assigning physical significance to small spectral shifts in either the CARS spectrum or the retrieved Raman spectrum in this regime is problematic, as the shifts may simply be due to the focusing conditions. The effects described here are generally limited to small regions of interest–those that lie within the Rayleigh range of the Gaussian beam. Larger homogenous samples that fill the entire Rayleigh range of the laser focus should not experience any such distortions.

There are a variety of approaches that one might take to disentangle the coupling in the system. Techniques that greatly suppress or eliminate the non-resonant background signal, such as interferometric CARS[25] and frequency modulation CARS[26] will push measurements into the limit of large $\chi_R^{(3)}$, and allow for direct study of the resonant response. Alternative NRB-free techniques such as SRS allow for similar measurements without these concerns as well. Finally, it should be noted that, as demonstrated in Figure 3c, if the retrieval algorithms are made aware of the phase shift in the spectrum, then it is possible to correct for this effect in post-processing.

ACKNOWLEDGMENTS

The authors would like to acknowledge the assistance of Dr. Chris Kingston of the NRC Emerging Technology Division for technical support and Dr. Erika Wee from the University of Ottawa Photochemistry Group for providing diamond samples. We would also like to acknowledge discussions with Dr. Adrian Pegararo from School of Engineering and Applied Science, Harvard University. Computations were performed on the Southern Ontario Smart Computing Innovation Platform (SOSCIP) BlueGene/Q supercomputer at the University of Toronto SciNet HPC facility. Financial support for this work was provided by the Natural Sciences and Engineering Research Council of Canada (NSERC), the Ontario Ministry of Research and Innovation, and Mprime NCE Strategic Postdoctoral Fellowship Program.

REFERENCES

1. A. Volkmer, "Vibrational imaging and microspectroscopies based on coherent anti-Stokes Raman scattering microscopy," *J. Phys. D: Appl. Phys.* **38**, R59-R81 (2005).
2. J. Cheng and X. S. Xie, "Coherent Anti-Stokes Raman Scattering Microscopy: Instrumentation, Theory, and Applications," *J. Phys. Chem. B* **108**, 827-840 (2004)
3. R. Burruss, A. D. Slepkov, A. F. Pegararo, and A. Stolow. "Unraveling the complexity of deep gas accumulations with three-dimensional multimodal CARS microscopy," *Geology* **40**, 1063-1066, (2012).
4. P.D. Maker and R.W. Terhune. "Study of optical effects due to an induced polarization thrid order in the electric field strength," *Phys. Rev.* **137** A801-18, (1965).
5. A. Zumbusch, G. R. Holtom, and X. S. Xie, "Three-Dimensional Vibrational Imaging by Coherent Anti-Stokes Raman Scattering," *Phys. Rev. Lett.* **82**, 4142-4145 (1999).
6. H-W. Wang, T.T. Le, J. Cheng, "Label-free Imaging of Arterial Cells and Extracellular Matrix Using a Multimodal CARS Microscope," *Opt. Commun.* **281** 1813-1822, (2008).
7. S. Maeda, T. Kamisuki, and Y. Adachi., in *Advances in Non-linear Spectroscopy*, edited by R. J. H. Clark and R. E. Hester. John Wiley and Sons Ltd., New York, (1988).
8. M.D. Levenson and N. Bloembergen. "Dispersion of the nonlinear optical susceptibility tensor in centrosymmetric media," *Phys. Rev. B.* **10**, 4447 (1974).
9. Y. Liu, Y.J. Lee, and M.T. Cicerone, "Broadband CARS spectral phase retrieval using a time-domain Kramers-Kronig transform," *Opt. Lett.* **34**, 1363 (2009)
10. E.M. Vartiainen, H.A. Rinia, M.M., and M. Bonn, "Direct extraction of Raman line-shapes from congested CARS spectra," *Opt. Express* **14**, 3622 (2006)
11. L. Li, H. Wang, and J. Cheng, "Quantitative Coherent Anti-Stokes Raman Scattering Imaging of Lipid Distribution in Coexisting Domains" *Biophys. J.* **89**, 3480 (2005)
12. M. Mu̇ller and J. M. Schins, "Imaging the Thermodynamic State of Lipid Membranes with Multiplex CARS Microscopy," *J. Phys. Chem.* **106**, 3715 (2002)
13. S.H. Parekh, Y.J. Lee, K.A. Aamer and M.T. Cicerone, "Label-free ceullular imaging by broadband coherent anti-Stokes Raman Scattering," *Biophys. J.* **99**, 2695 (2010)
14. E.O. Potma, W.P. de Boeij, and D.A. Wiersma, "Nonlinear coherent four-wave mixing in optical microscopy," *J. Opt. Soc. Am. B*, **17**, 1678, (2000)
15. J. Cheng, A. Volkmer, and X.S. Xie, "Theoretical and experimental characterization of coherent anti-Stokes Raman scattering microscopy," *J. Opt. Soc. Am. B*, **19**, 1363 (2002)
16. N. Djaker, D. Gachet, N. Sandeau, P.-F. Lenne, and H. Rigneault, "Refractive effects in coherent anti-Stokes Raman scattering microscopy," *App. Opt.* **45**, 7005 (2006)
17. K.I. Popov, A. F. Pegoraro, A. Stolow, and L. Ramunno, "Image formation in CARS microscopy: effect of the Gouy phase shift," *Opt. Express* **19**, 5904 (2011)
18. A. F. Pegoraro, A. D. Slepkov, A. Ridsdale, D. J. Moffatt, and A. Stolow, "Hyperspectral multimodal CARS microscopy in the fingerprint region," *J. Biophot.* in press (2012)
19. T. Hellerer, A. M. Enejder, and A. Zumbusch, "Spectral focusing: High spectral resolution spectroscopy with broad-bandwidth laser pulses," *Appl. Phys. Lett.* 85, 2527 (2004).
20. S. A. Solin and A. K. Ramdas, "Raman spectrum of diamond," *Phys. Rev. B* **1**, 16871698 (1970).
21. C.V Stephenson, W.C Coburn Jr., and W.S Wilcox, "The vibrational spectra and assignments of nitrobenzene, phenyl isocyanate, phenyl isothiocyanate, thionylaniline and anisole," *Spectrochimica Acta* **17**, 933 (1961)
22. M. Fujii, M. Tahara, I. Sakagami, W. Freude, and P. Russer, "High-order FDTD and auxiliary differential equation formulation of optical pulse propagation in 2D Kerr and Raman nonlinear dispersive media," *IEEE J. Quantum Electron.* **40**, 175 (2004)
23. K.S. Yee, "Numerical solution of initial boundary value problems involving Maxwell's equations in isotropic media," *IEEE Trans. Ant. Prop.* **AP-14**, 302 (1966)
24. D. Vanderbilt and S.G. Louie, "A Monte carlo simulated annealing approach to optimization over continuous variables," *J. Comput. Phys.* **56**, 259 (1984)

25. C.L. Evans, E.O. Potma, and X.S. Xie, "Coherent anti-Stokes Raman scattering spectral interferometry: determination of the real and imaginary components of nonlinear susceptibility $\chi(3)$ for vibrational microscopy" *Optics Letters*, **29**, 2923, (2004).
26. F.Ganikhanov, C.L. Evans, B.G. Saar, and X.S. Xie, "High-sensitivity vibrational imaging with frequency modulation coherent anti-Stokes Raman scattering (FM CARS) microscopy," *Optics Letters*, **31**, (2006).